



OPEN

Metallic one-dimensional heterostructure for gas molecule sensing

Prabal Dev Bhuyan^{1,2}, Sanjeev K. Gupta¹✉, Rajeev Ahuja^{3,4} & P. N. Gajjar²✉

We have investigated a new metallic core–shell nanowire (NW) geometry of that could be obtained experimentally, that is silicon (Si) and germanium (Ge) NWs with cores constituted by group-10 elements palladium (Pd) and platinum (Pt). These NWs are optimized with two different diameters of 1.5 Å and 2.5 Å. The nanowires having diameter of 1.5 Å show semi-metallic nature with GGA-PBE calculation and metallic nature while spin orbit interaction (SOC) is included. The quantum conductance of the NWs increases with the diameter of the nanowire. We have investigated current–voltage (IV) characteristics for the considered NWs. It has been found that current values in accordance with applied voltage show strong dependence on the diameter of the NWs. The optical study of the NWs shows that absorption co-efficient peak moves to lower energies; due to quantum confinement effect. Furthermore, we have extensively studied optical response of Pd and Pt based core–shell NWs in O₂ and CO₂ environment. Our study on Si and Ge based metallic core/shell NW show a comprehensive picture as possible electron connector in future nano-electronic devices as well as nano gas detector for detecting O₂ gas.

The rising environmental concerns and the effect of pollution on health call lead to worldwide problem. As a result gas sensing has become as field of continuous research to detect industrial and automobile emissions and for monitoring our environment and household safety. These concerns have led to recommendations on the development of high performance gas sensors with high sensitivity and selectivity^{1,2}. The sensing sensitivity can be enhanced by increasing the contact interface between the gas molecules and sensing materials³. Therefore, one dimensional (1D) nanomaterials are considered to be promising material with high sensitivity and selectivity due to large surface to volume ratio and enormous reaction sites⁴.

In this regard, the 1D materials have synthesized and showed potential application as gas sensing material⁴. The change in conductivity of gold (Au) nanowire with the gas molecules shows the potential for gas sensor^{4,5}. Beyond Au-NW, metal nanowires such as silver (Ag)⁶, palladium (Pd)^{7,8} have also been studied and developed as sensors. Silicon (Si) nanowire has also attracted much attention as for ultra-fast chemical sensing systems^{9,10}. A. Miranda and coworkers have reported the change in band gap upon the adsorption various gas molecules on the surface of Si-NW attributes its application in the field of sensing⁹. In addition, it is observed that nanowires combined with metal nanoparticles, enhances the reacting properties of the materials due to their unique chemical and physical properties^{11–13}. Beyond that, heterostructure core–shell nanowires are also studied and synthesized for detecting gas molecules. Dong Liu et al. have created lower power consumption gas sensor from Si–TiO₂ core–shell NW and successfully demonstrated sensing performance for CH₄ detection at room temperature¹⁴. Further, Daejong Yang et al. have fabricated flexible gas sensor based on ZnO/ZnS core–shell NW³.

However, silicon (Si) and germanium (Ge) nanowires with cores constituted by transition metal group-10 element Pd and Pt have not been exploited yet. Both Pd and Pt nanowires have been synthesized experimentally and gained a high interest^{15,16}. Pd nanowire has shown applications in the field of sensing as hydrogen detector^{8,17}. Similarly, it has been reported that Pt nanowire could find applications as electro-catalysts in proton exchange fuel cells, high performance hydrogen sensors etc.^{18,19}. Therefore, we intend to explore the electronic and optical properties of the Si and Ge shell based Pd and Pt core nanowire systems for gas detection.

¹Computational Materials and Nanoscience Group, Department of Physics and Electronics, St. Xavier's College, Ahmedabad 380009, India. ²Department of Physics, University School of Sciences, Gujarat University, Ahmedabad 380009, India. ³Condensed Matter Theory Group, Department of Physics and Astronomy, Uppsala University, Box 516, 75120 Uppsala, Sweden. ⁴Applied Materials Physics, Department of Materials and Engineering, Royal Institute of Technology (KTH), 100 44 Stockholm, Sweden. ✉email: sanjeev.gupta@sxca.edu.in; pngajjar@gujaratuniversity.ac.in

In this work, we have focused on Si or Ge based metallic Pd- and Pt-core/shell nanowires and studied their geometry and electronic properties. Diameter dependent I–V characteristics and optical properties are also investigated in order to provide a picture as comprehensive as possible. Furthermore, we have adsorbed O₂ and CO₂ gas molecules on the considered core–shell nanowires to study the response of the nanowires with gas molecules and highlighted the optical sensitivity to investigate the suitability of the nanowires as a gas sensor.

Methodology

Our present calculations are based on density functional theory (DFT) methods using SIESTA package for electronic structure and transport properties²⁰. Generalized gradient approximation (GGA) using Perdew–Burke–Ernzerhof (PBE) is adopted for the exchange and correlational functional²¹. We have used Troullier–Martins norm-conserving and relativistic pseudopotential to account for core electrons and double zeta polarized basis set to describe valence electrons²². The ground state nanowire geometries are relaxed with conjugate gradient (CG) algorithm. Convergence on the density matrix during a self-consistent cycle was set to 10^{−6} eV. We have considered sufficient vacuum of 20 Å in x and y-direction to avoid interaction between the neighboring nanowire images. The reciprocal space is sampled at 1 × 1 × 12 using Monkhorst Pack meshes. We include 30 K-points in the band structure along Γ to Z.

The current–voltage (IV) characteristics graph of the optimized structure have been calculated by using non-equilibrium Green's function (NEGF) technique, with Keldysh formalism based on density functional theory²³. A two probe system is designed to study the IV properties of the core–shell NW confined in the central scattering region (SR) contact with semi-infinite left electrode (LE) and right electrode (RE). We have considered both electrodes and SR are made of the same material. Our goal is to compute transmission function, which can be obtained from the Green's function of the system. The transmission function T(E) is given by²⁴,

$$T(E) = \text{Tr}[G(E)\Gamma_R(E)G(E)\Gamma_L(E)] \quad (1)$$

$\Gamma_L(E)$ and $\Gamma_R(E)$ are the broadening matrices. G(E) is the Green's function. The Green's function G(E) of the SR is calculated from the formula,

$$(ES - H)G(E) = I \quad (2)$$

where, S is the overlap matrix, H is the Hamiltonian and I is the identity matrix. The Hamiltonian is composed of as follows,

$$\begin{pmatrix} H_L + \sum_L & H_{LC} & 0 \\ H_{LC} & H_C & H_{RC} \\ 0 & H_{RC} & H_R + \sum_R \end{pmatrix}$$

Here, L, C and R denote the left electrode, central region and right electrode, respectively. \sum_L and \sum_R are the self-energies for the two electrodes.

From transmission function, the current through the contact region is calculated,

$$I(V_{bias}) = G_0 \int_{\mu_R}^{\mu_L} T(E, V_{bias}) dE \quad (3)$$

where, $G_0 = 2e^2/h$ is the unit of quantum conductance and $T(E, V_{bias})$ is the transmission probability of the electron incident with an energy E through the device under the potential bias V_{bias} . The bias voltage between the two electrodes of different electrochemical potential μ_L and μ_R is given by $eV_{bias} = \mu_L - \mu_R$.

Further, we have investigated the optical properties of the NWs for the both diameters and analyzed the variation of the properties with gas adsorbed NWs for sensing application. We have considered only interband transition for the optical properties calculation. The frequency dependent complex dielectric function can be written as $\epsilon = \epsilon_1 + i\epsilon_2$. ϵ_1 is the real part of the dielectric function and is determined from the Kramers–Kronig (KK) relationship. ϵ_2 is the imaginary part of the function is obtained from the summation over electronic states. The ϵ_2 depicts the absorption behaviour of the material, which can be written as;

$$\alpha(\omega) = \sqrt{2}\omega \left[\{ \epsilon_1^2(\omega) + \epsilon_2^2(\omega) \}^{1/2} - \epsilon_1(\omega) \right]^{1/2} \quad (4)$$

Results and discussions

Structure and stability. We have considered two different cores; palladium (Pd) and platinum (Pt), which are wrapped by germanium (Ge) and silicon (Si) shell. Therefore, we have four different core–shell NW configurations: Pd_{core}/Ge_{shell}, Pt_{core}/Ge_{shell}, Pd_{core}/Si_{shell} and Pt_{core}/Si_{shell}. The surface of the NWs is passivated by hydrogen atom to prevent dangling bond. The relaxed and optimized geometry of core–shell NWs are shown in Fig. 1. The core of the considered core–shell NWs is constituted with 6 atoms of Pd or Pt and the thickness of the Si or Ge shell is varied with nanowire size. Considering Pd/Ge NW, the core wrapped by one monolayer (1ML) of Ge shell has 40 atoms (6 Pd atoms, 18 Ge atoms and 16 H atoms) with a diameter of ~1.5 nm. The diameter increases to ~2.3 nm while the core is wrapped by 2MLs of Ge shell with 78 atoms (6 Pd atoms, 48 Ge atoms and 24 H atoms). The core with 1ML shell is denoted by 1R (Fig. 1a) and with 2ML shells is denoted by 2R (ESI, Figure S1a). The NWs are considered along the [110] direction, which is reportedly preferred growth direction

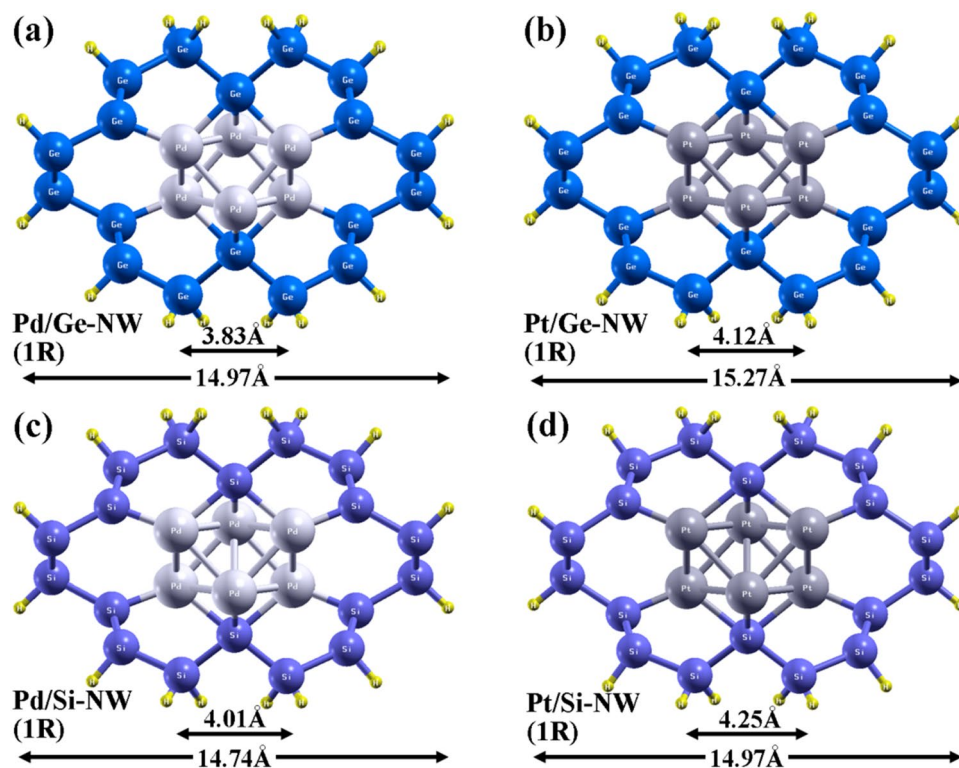


Figure 1. Front view of the fully optimized structures of (a) Pd/Ge, (b) Pt/Ge, (c) Pd/Si and (d) Pt/Si core-shell NWs. The core is wrapped by 1ML Ge or Si-shell. Hydrogen atoms are passivated on the surface of the NWs to prevent the dangling bonds.

Core-shell NW	Pd/Ge		Pt/Ge		Pd/Si		Pt/Si	
	1R	2R	1R	2R	1R	2R	1R	2R
E_{coh} (eV/atom)	-3.68	-3.80	-3.66	-3.79	-4.16	-4.43	-4.14	-4.42
Quantum conductance (G_0)	2	12	2	10	2	10	2	14

Table 1. Cohesive energy (E_{coh}) and quantum conductance of the considered core-shell NWs.

in case of synthesized Si NW and also Ge/Si core-shell NW²⁵. We have observed that the variation in diameter of the NWs is according to the radius of atoms also.

In order to comprehend the energetic stability of the morphology, we have calculated cohesive energy of the NWs from the following equation;

$$E_{coh} = \frac{E_T - nE_a}{n} \quad (5)$$

where, E_T is the total energy of the core-shell NW, E_a is the energy of a free atom and n is the total number of atoms in the nanowire. We have obtained negative cohesive energy for the core-shell nanowires (see in Table 1). The negative values of cohesive energy (E_{coh}) indicates the stability of the nanowires. It is observed that E_{coh} increases with the diameter of the respective nanowire. The NWs shows cohesive energy in the range of $-3.6 \sim -3.8$ eV, while Pd and Pt core wrapped with Ge shell. The energy range decrease to $-4.1 \sim -4.4$ eV, while Pd and Pt core wrapped with Si shell. It is reported that pure Pd-NW having diameter of 2.57 Å shows cohesive energy of ~ -2.4 eV and Pt-NW having diameter of 2.61 Å shows cohesive energy of ~ -4.2 eV²⁶.

Electronic properties. After the structural optimization, we have focused on the electronic properties of these core-shell nanowires. We have studied both the with spin-orbit interaction and the without spin orbit interaction electronic band structure. The electronic band structures of 1R and 2R NWs are shown in Figs. 2 and 3, respectively.

The core-shell NW with 1ML (1R) shows semi-metallic behaviour without spin-orbit interaction calculation as a single Fermi level crossing near the zone boundary. The electronic band structure shows that $2G_0$ quantum conductance as the bands line touches the Fermi energy level at two points near the Z-point. However, Pd/Ge and Pt/Ge NW shows metallic behaviour with quantum conductance of $4G_0$, while spin-orbit interaction is included.

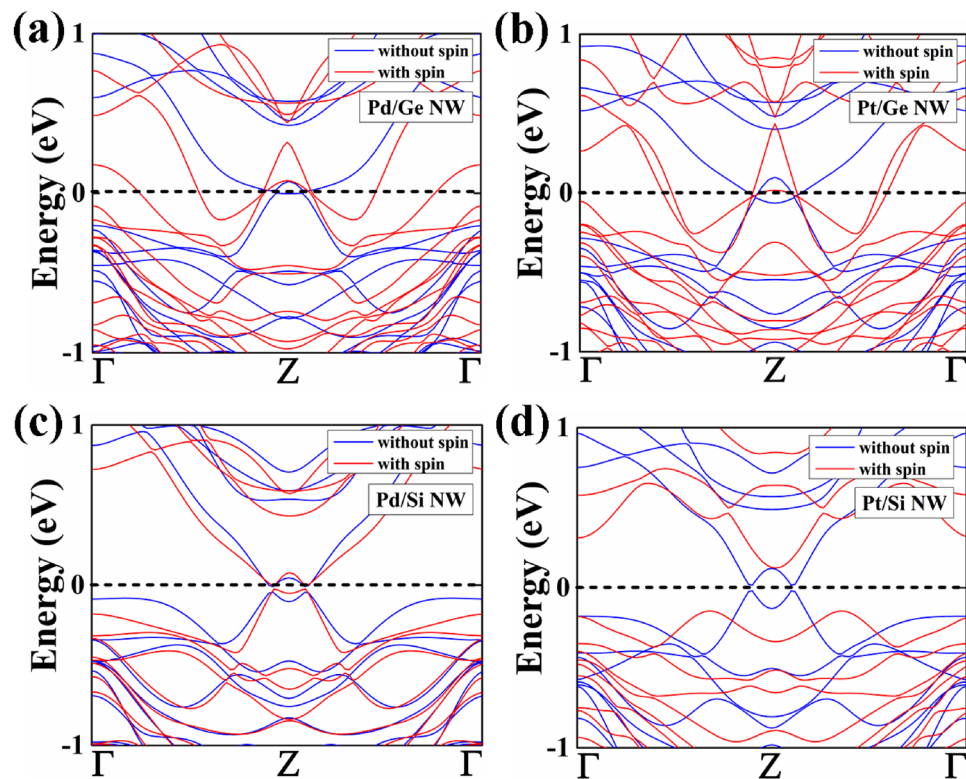


Figure 2. The electronic band structure without spin–orbit interaction and within spin–orbit interaction of (a) Pd/Ge, (b) Pt/Ge, (c) Pd/Si and (d) Pt/Si NWs having diameter of 1.4–1.5 nm (1R) is shown. The Fermi level is set at 0 eV.

Pd/Si NW shows similar semimetallic behaviour from both the with spin–orbit interaction and the without spin–orbit interaction calculation. In case of Pt/Si NW, there is a band gap of 0.26 eV appears at the Fermi level (E_f) which shows semiconducting behaviour using spin–orbit interaction. Furthermore, we have found that the increase in the diameter of core–shell NWs results in the transition of electronic properties. The Pd and Pt core wrapped by 2ML Ge and Si shell NWs show metallic nature, which means resistivity decreases with the diameter. The decreasing resistivity with increasing nanowire diameter is explained by Fuchs–Sondheimer (FS) theory. As the size of our considered core–shell nanowires are shorter than the mean free path of the electron, therefore, the surface scattering influences the resistance of a nanowire^{27,28} which leads to the decrease in resistivity. Pd/Ge and Pt/Si NW show conductance of $12G_0$ and $14G_0$, respectively from both the with and without spin orbit interaction. Though both the NWs show same conductance value, but the change in electronic band structure is observed near the Fermi region. The other two nanowires Pt/Ge and Pd/Si NW shows variation in conductance for the spin orbit interaction and without spin orbit interaction calculation. Pt/Ge NW shows conductance of $8G_0$ ($10G_0$) under spin orbit interaction (without spin orbit interaction). Further, Pd/Si NW shows conductance of $6G_0$ ($14G_0$) under spin orbit interaction (without spin orbit interaction). So, we have observed that as the diameter of the nanowires decreases, the band gap is increased. The increase of band gap is due to the quantum confinement effect.

To study the orbital contribution of the nanowires near the Fermi energy level, we have studied the partial density of states and are shown in ESI (Figure S2 and S3). The contribution of both core and shell is observed near the Fermi energy. In the case of 1R NWs, the core, Pd-4d and Pt-5d orbital electron are more dominant than the shell region on the valence band. However, at the conduction band, the contribution of the shell region; Ge-4p and Si-3p orbital is observed to be higher. The contribution of orbitals notably changes as the diameter of the NWs increases from 1 to 2R. It is observed that both the valence band and conduction band is largely contributed by the shell region. The Ge-4p and Si-3p are actively dominant near the Fermi energy level. Thus, the Si and Ge shells of different thicknesses lead to a tuning of the electronic structure of the Pd and Pt nanowires through a state of hybridization between the core and shell orbitals at the interface.

We have observed that quantum conductance of the core–shell NWs increases with increase in diameter. To support the electronic structure study, we have studied the I–V characteristics of the core–shell NWs using NEGF technique as discussed in methodology section. We have considered a two probe system of electrodes (LE and RE) and scattering region (SR). The length of the SR is 12–13 Å with three primitive unit cells and is sufficient enough to avoid an abrupt change in electronic structure. We have increased V_{bias} in the steps of 0.1 V and used converged density matrix of the previous step as the initial guess for the next step. By applying a bias voltage, the Fermi level of the left electrode shifts with respect to the Fermi level of the right electrode. While, the energy of

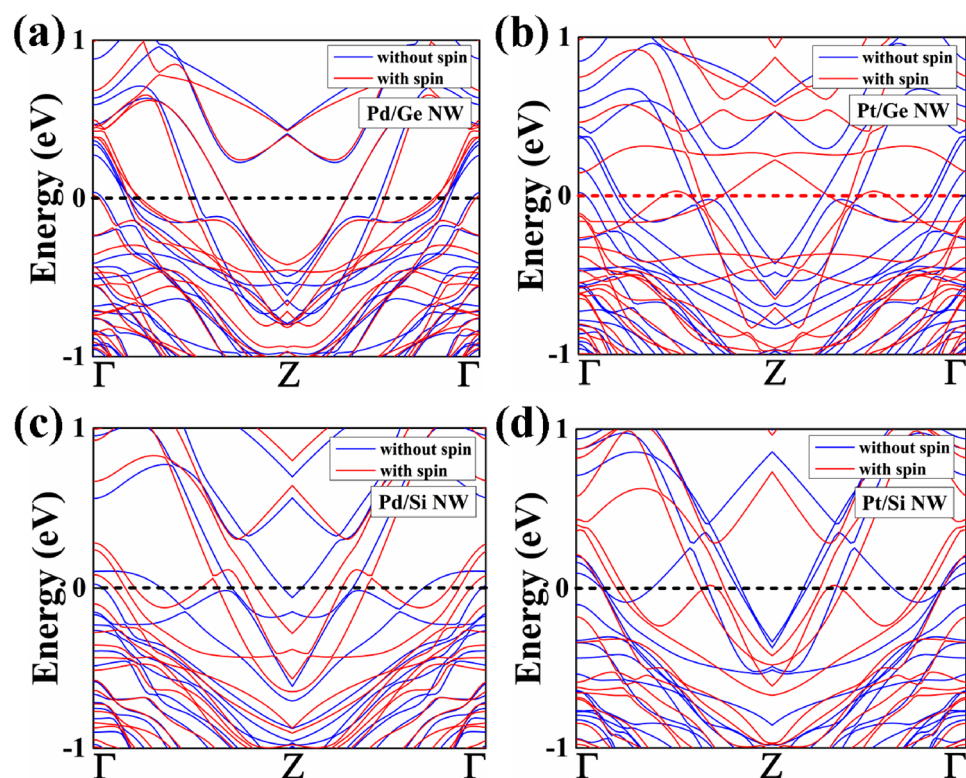


Figure 3. The electronic band structure without spin–orbit interaction and within spin–orbit interaction of (a) Pd/Ge, (b) Pt/Ge, (c) Pd/Si and (d) Pt/Si NWs having diameter of 2.2–2.3 nm (2R) is shown. The Fermi level is set at 0 eV.

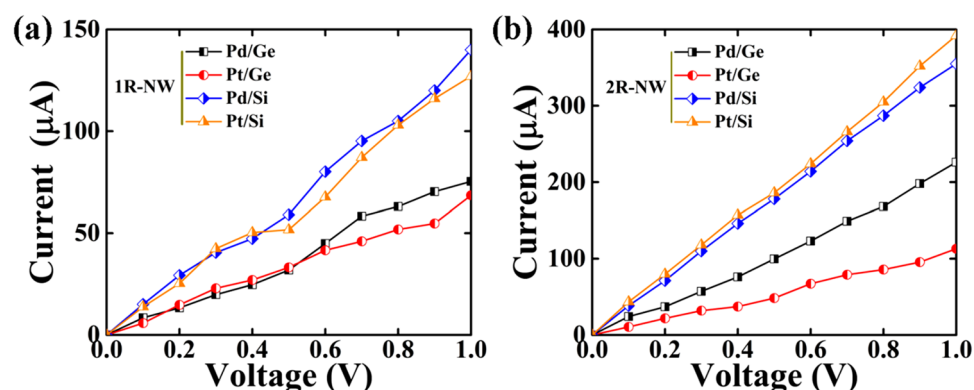


Figure 4. Current–Voltage (I–V) plot for (a) 1R and (b) 2R core–shell NWs for bias voltages from 0 to 1 V.

the top of the valance band of the left electrode matches with the energy of the bottom of the conduction band of the right electrode, the current starts flowing through the system. The current as a function of the applied bias voltage (V_{bias}) is present in Fig. 4.

We have observed that the Pd and Pt cores wrapped by 1ML wide Ge and Si shells show linear I–V characteristics behaviour as shown in Fig. 4a. The value of current passing through the SR increases linearly with applied voltage. The cores wrapped with Si-shell show higher current value than Ge-shell at corresponding applied voltage. The current is calculated to 140 μA and 127 μA for Pd/Si (1R) and Pt/Si (1R), respectively at 1.0 V, while the Pd/Ge and Pt/Ge shows the current value of 75.3 μA and 68.5 μA , respectively. It is also observed that these NWs show a high magnitude of current at corresponding applied voltage comparing to Sb²⁹, As²⁹ and Ni³⁰ core, wrapped with same shell material and same diameter.

Further, when the core is wrapped 2ML wide shell, the magnitude of current of the core–shell NWs abruptly increases, as shown in Fig. 4b. Both Pd/Si (2R) and Pt/Si (2R) NWs show an increment of current of around 180% and reach 355 μA and 392 μA , respectively for applied voltage 1.0 V. The current value for Pd/Ge (2R) and Pt/Ge (2R) NW increases upto 226 μA and 113 μA at applied voltage 1.0 V, respectively as the shell diameter increases.

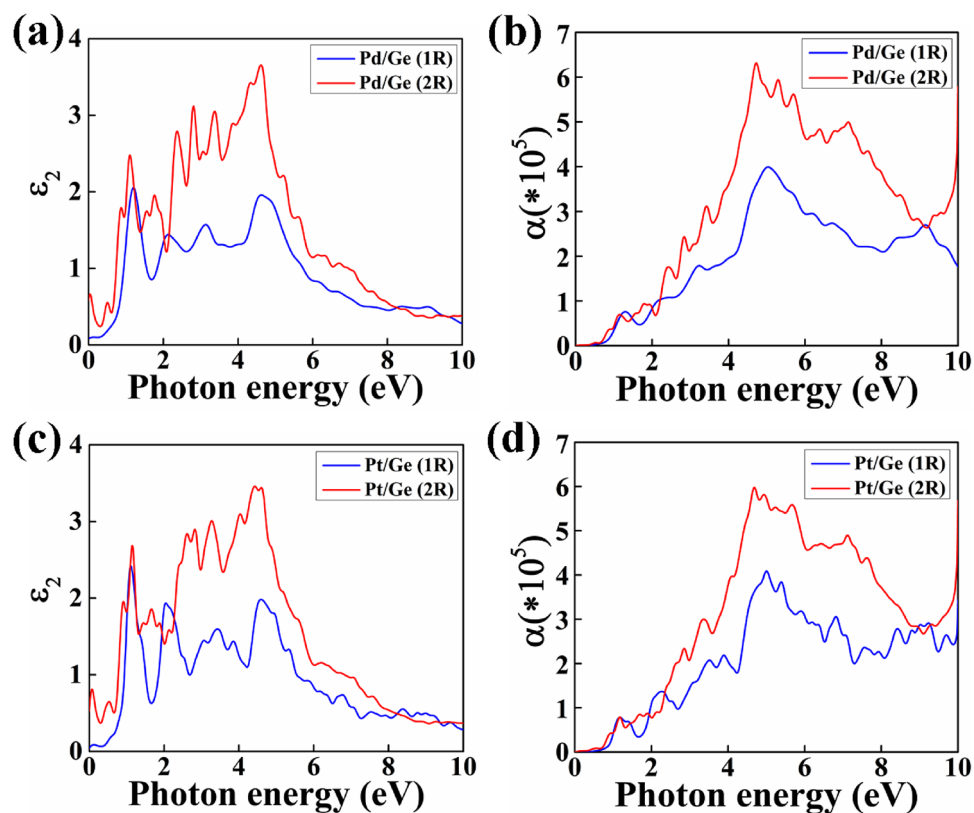


Figure 5. The diameter dependent imaginary part of the dielectric constant (ϵ_2) with photon energy and its corresponding adsorption co-efficient are shown in (a,b) for Pd/Ge and (c,d) for Pt/Ge core/shell NW.

The increasing current value corresponding to applied voltage with increasing the diameter of the NW leads to decrease in resistivity of the NW. This phenomenon can be explained by Fuchs–Sondheimer (FS) theory, as the size of our core–shell NWs is shorter than the mean free path of the electron, therefore surface scattering will influence the resistance of the NW, which leads to decrease in resistivity^{27,28}.

Optical properties. The imaginary part (ϵ_2) of the frequency dependent complex dielectric function can be described by the electronic band structure of the material and is related to the absorption spectra. We have investigated the optical properties of the nanowires in plane (E||Z) polarization of light. The observed peaks in the ϵ_2 graph provide the information about the interband transitions of electron corresponding to the photon energy from occupied states to unoccupied states of the band structure. The ϵ_2 of the NWs are shown in Figs. 5a,c and 6a,c. We have observed a valley region upto 1 eV for all the NWs having diameter of 1R.

However, in case of NWs with 2R diameter, sharp peaks have been observed in that valley region. These peaks are obtained due to the metallic behaviour of the NWs with 2R diameter. We can clearly observe the transition from semi-metallic to metallic behaviour in ϵ_2 graph due to the transition of electrons.

Further, we have studied absorption coefficient of the NWs to analyze their potential in optical device applications. It provides the information of the rate at which intensity of light decreases as it passes through the material. These core/shell NWs show high absorption co-efficient in the ultraviolet (UV) range and the absorption co-efficient increases with increase in diameter of the NWs as shown in Figs. 5b,d and 6b,d. This absorption co-efficient of the material depends on the imaginary part (ϵ_2) of the frequency dependent complex dielectric function. High absorption co-efficient of $3.9 \times 10^5 \text{ cm}^{-1}$ is obtained at 5.04 eV for Pd/Ge NW with 1R diameter. However, as the diameter of the NW increase to 2R, the absorption co-efficient red shifted to 4.69 eV and the value increases to $6.25 \times 10^5 \text{ cm}^{-1}$. Similarly, Pt/Ge (1R) shows highest peak at 4.99 eV of $4.0 \times 10^5 \text{ cm}^{-1}$ and increases to $5.98 \times 10^5 \text{ cm}^{-1}$ at 4.68 eV for 2R diameter. The Pd/Si (1R) and Pt/Si (1R) NWs exhibit absorption co-efficient of $4.68 \times 10^5 \text{ cm}^{-1}$ at 5.71 eV and $4.41 \times 10^5 \text{ cm}^{-1}$ at 5.49 eV, respectively. The value of co-efficient changes to $6.53 \times 10^5 \text{ cm}^{-1}$ at 5.42 eV for Pd/Si (2R) and $6.54 \times 10^5 \text{ cm}^{-1}$ at 5.41 eV for Pt/Si (2R) NW. The peaks move to lower energies as diameter increases is due to quantum confinement effect³¹.

Nanowire as optical sensor. Gas detection has become as field of continuous research to detect industrial and automobile emissions and for monitoring our environment and household safety. In this regard, metallic NWs like, Au³² and Pd¹⁷ have shown great possibility in the field of gas sensing. This motivates us to investigate the optical response of Pd and Pt based core–shell NWs in O₂ and CO₂ environment.

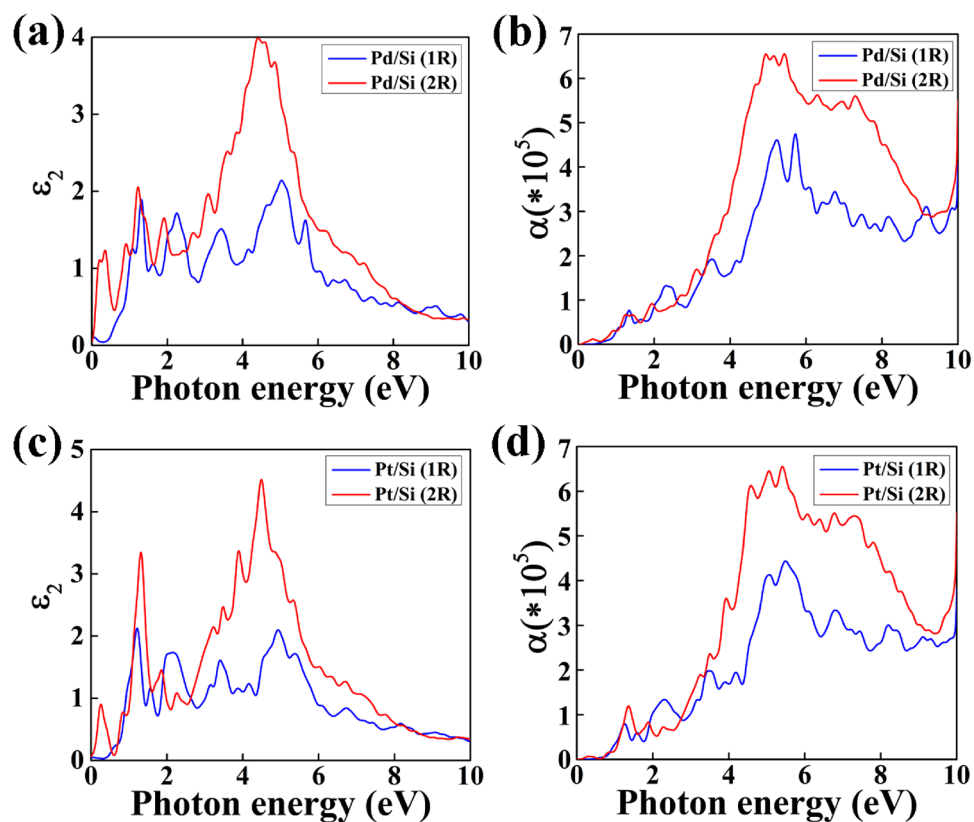


Figure 6. The diameter dependent imaginary part of the dielectric constant (ϵ_2) with photon energy and its corresponding adsorption co-efficient are shown in (a,b) for Pd/Si and (c,d) for Pt/Si core/shell NW.

Adsorption of gas molecules. In this section, we have focused our study on the effect of adsorption gas molecules on the optical properties of the core-shell nanowires. To reveal the possibilities of Pd and Pt core-shell NW based sensors, it is important to understand the interaction between the NW and adsorbent gas molecules. We have considered two types of configuration gas molecule geometry, represented by 1 and 2 as shown in Fig. 7a,b. We have adsorbed O_2 and CO_2 gas molecules on the $(1 \times 1 \times 3)$ supercell of 1R core-shell NW as shown in Fig. 7c. The gas molecules are placed on the surface of the NW at a distance of 1.5 \AA . After relaxation, gas molecules are observed to be changed their positions as shown in Figures S4, S5. The distance between the gas molecule from the surface of the NW after relaxation are detailed in Table 2. The change in their positions and structure of gas molecules is observed due to the interaction between two. According to these changes, we have calculated adsorption energy and relaxation time of the molecules.

The adsorption energy of the gas molecules on the NW is calculated from the equation;

$$E_{ads} = E_{adsorbed-NW} - (E_{core/shell} + E_{adsorbent-gas}) \quad (6)$$

where, $E_{adsorbed-NW}$ is the total energy of the gas molecule adsorbed on the core-shell NW, $E_{core/shell}$ is the total energy of the respective core-shell NW and $E_{adsorbent-gas}$ is the total energy of the respective gas molecule. We have observed that CO_2 gas molecules on core-shell NW show adsorption energy of $-0.18 \sim -0.22 \text{ eV}$. However, O_2 gas molecule shows comparatively higher adsorption energy of $-0.45 \sim -0.65 \text{ eV}$. It is noticed that the type 1 geometry of O_2 gas molecule on Pd/Si-NW shows highest adsorption energy of -0.65 eV as shown in Table 2. Another important feature to study is the relaxation time of the molecules, which gives information about the sustaining time period of gas molecules on the NWs. The relaxation time is calculated by;

$$\tau \approx \exp(-E_{ads}/K_B T) \quad (7)$$

where, E_{ads} is the calculated adsorption energy, K_B is the Boltzmann constant and T is the temperature. We have considered temperature to be 300 K in this calculation. As the relaxation time is directly proportional to the adsorption energy, we have observed that relaxation time for O_2 gas molecule on the NW is greater the CO_2 gas. Similarly, the type 1 geometry of O_2 gas on Pd/Si NW shows maximum relaxation time of 7.9×10^{10} .

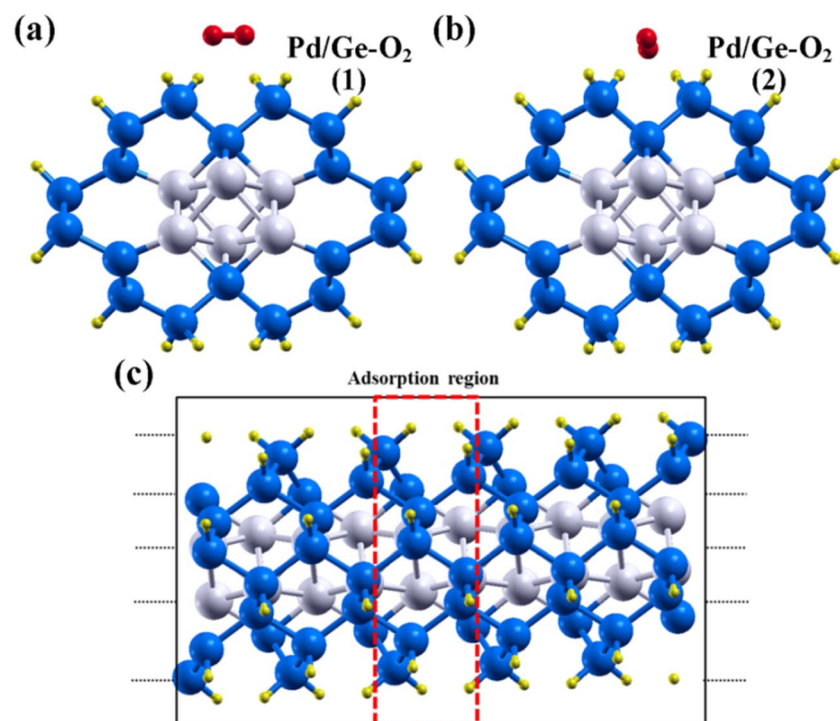


Figure 7. Relaxed O_2 gas molecules on Pd/Ge-NW having configuration (a) type 1 geometry and (b) type 2 geometry. Schematic view of NW system having 5 primitive cells along the z-axis is shown in figure (c).

Nanowire	Adsorbed gas molecules	Position of the molecules	Distance between the nanowire and gas molecules (Å)	Adsorption energy (eV)	Relaxation time
Pd/Ge	CO_2	1	2.79	-0.18	1.0×10^3
		2	2.62	-0.20	2.2×10^3
	O_2	1	2.32	-0.45	3.5×10^7
		2	2.02	-0.56	2.4×10^9
Pt/Ge	CO_2	1	2.58	-0.19	1.5×10^3
		2	2.70	-0.21	3.3×10^3
	O_2	1	2.08	-0.50	2.4×10^8
		2	1.99	-0.51	3.6×10^8
Pd/Si	CO_2	1	2.66	-0.20	2.2×10^3
		2	2.60	-0.20	2.2×10^3
	O_2	1	2.10	-0.65	7.9×10^{10}
		2	1.98	-0.62	2.5×10^{10}
Pt/Si	CO_2	1	2.70	-0.20	2.2×10^3
		2	2.61	-0.22	4.9×10^3
	O_2	1	2.30	-0.43	1.6×10^7
		2	1.99	-0.57	3.6×10^9

Table 2. Calculated distance between the nanowire and gas molecules, adsorption energy and relaxation time of the gas molecules.

Electronic properties. The study of electronic properties of the gas adsorbed nanowire is very important to understand the interaction between them; therefore, we have computed projected density of states (PDOS) to analyze the contribution gas molecules near the Fermi energy level and are shown in Figs. 8, 9 and Figure S6 and S7.

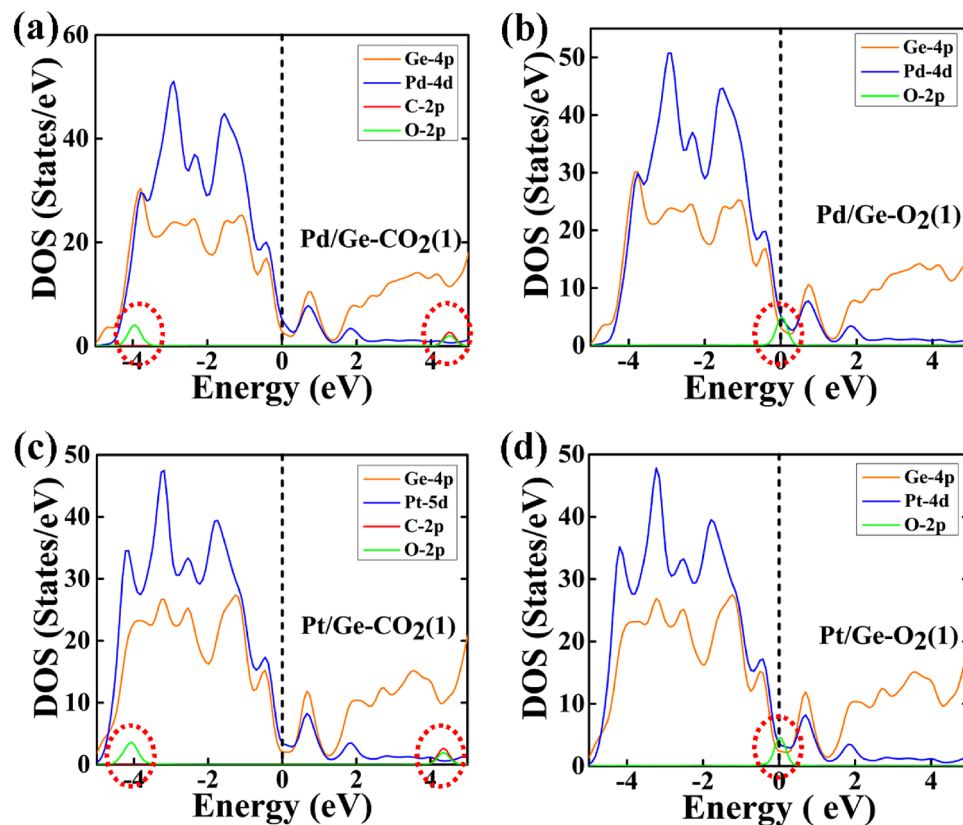


Figure 8. The partial density of states (PDOS) of type 1 geometry of CO₂ and O₂, are adsorbed on Pd/Ge and Pt/Ge core-shell NW: (a) CO₂ adsorbed Pd/Ge NW, (b) O₂ adsorbed Pd/Ge NW, (c) CO₂ adsorbed Pt/Ge NW and (d) O₂ adsorbed Pt/Ge NW. The Fermi energy is set at 0 eV.

The contribution of O₂ gas molecules is observed at the Fermi energy level. Therefore, O₂ gas molecule shows stronger adsorption energy and higher relaxation time than CO₂ molecule. Another smaller peak of O₂ is also observed near the Fermi levels in the range of 0.65–0.75 eV, which is not visible in Figs. 8 and 9. In the case of CO₂ adsorbed core-shell nanowires, the PDOS reveals the contribution of O-2p orbitals of CO₂ in the valance band from ~ -3.5 eV to ~ -4.5 eV. However, at conduction band, the contribution of CO₂ is observed due to the hybridization of C-2p and O-2p orbital in the range from ~ 4.0 eV to ~ 4.7 eV. The range and states/eV of O₂ and CO₂ contribution slightly changes with different core-shell NW and geometry of the gas molecules.

Effect on optical properties. We have clearly observed that CO₂ gas molecules adsorbed on NWs shows absorption energy in the range of -0.18 ~ -0.22 eV. It is reported that the interaction between the gas molecules and the substrate should be in the scale of -0.5 eV for effective sensing³³. Therefore, we will focus on O₂ gas molecules adsorbed on the core/shell NWs as the absorption energies are in the range of -0.45 ~ -0.65 eV.

We have analyzed imaginary part (\mathcal{E}_2) of the dielectric function of O₂ gas adsorbed NWs and compared the results with pure one as shown in Fig. 10. We have calculated the imaginary part for the both type 1 and 2 geometry configuration of O₂ gas molecules. From Fig. 10a, we have observed a valley region upto 1 eV, there are no sharp peaks. However, in presence of O₂ gas molecules, the Pd/Ge core/shell NW shows a peak at 0.007 eV for type 1 geometry configuration and at 0.11 eV for type 2 geometry configuration. The contribution of O₂ gas molecule is observed in infra-red (IR) region. We have observed no change in optical properties in the visible and ultraviolet (UV) range. The extra peak observed in the IR region is due to O-2p states electronic contribution at the Fermi energy level as shown in Fig. 8b and ESI, Figure S6 (b). Similarly, we have observed imaginary part peak for O₂ adsorbed Pt/Ge NW at IR-region due O-2p states electron contribution as comparison to flat valley for pure NW (Fig. 10b). In case of Pd/Si NW, two peaks are observed at 0.16 eV and 0.55 eV for type 1 position and at 0.04 eV and 0.37 eV for type 2 configuration of O₂ gas (Fig. 10c). There is no change in optical properties of Pd/Si-NW in the visible and ultraviolet (UV) range in presence of O₂ gas molecule. We have also observed two peaks for O₂ adsorbed Pt/Si-NW. The contribution of O₂ gas is observed at 0.08 eV and 0.40 eV for type 1 and at 0.09 eV and 0.43 eV for type 2 configuration as shown in Fig. 10d. It can be clearly noted that the change

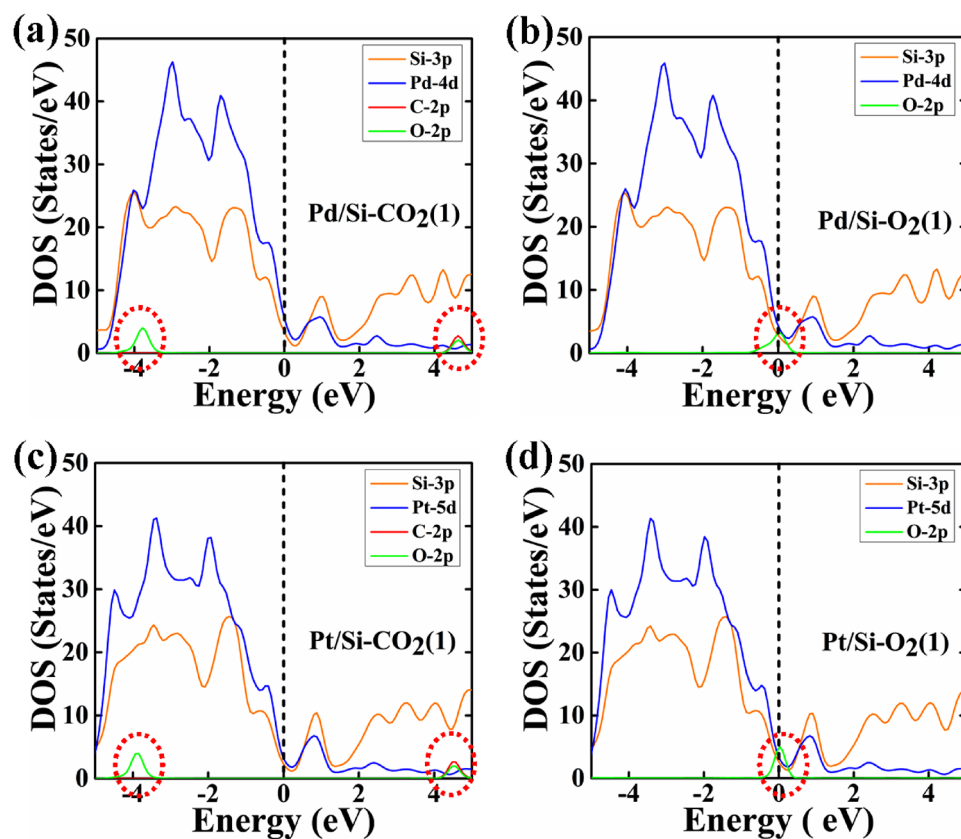


Figure 9. The partial density of states (PDOS) of type 1 geometry of CO_2 and O_2 , are adsorbed on Pd/Si and Pt/Si core-shell NW: (a) CO_2 adsorbed Pd/Si NW, (b) O_2 adsorbed Pd/Si NW, (c) CO_2 adsorbed Pt/Si NW and (d) O_2 adsorbed Pt/Si NW. The Fermi energy is set at 0 eV.

in optical properties in core-shell NWs is observed at IR region due to the O-2p orbital electron contribution at the Fermi energy level. The optical properties of the core/shell NWs indicate that these have great potential applications in optical gas sensors for sensing O_2 gas in the IR region.

Conclusions

In this work, we have investigated a new metallic core-shell nanowire geometry of that could be obtained experimentally, that is silicon (Si) and germanium (Ge) nanowires with cores constituted by group-10 element Pd and Pt. We have fully optimized four different core-shell NW configurations and negative values of cohesive energy (E_{coh}) indicates the stability of the nanowires. The electronic band structure properties show transition from semi-metallic to metallic behaviour with the diameter of the nanowire. The linear current-voltage (IV) characteristics of the NWs indicate ohmic behaviour and it has been found that current values in accordance with applied voltage show strong dependence on the diameter of the NWs. We have also studied diameter dependent optical properties. The absorption co-efficient peaks move to lower energies is due to quantum confinement effect. Furthermore, the change in optical properties of the NWs in presence of O_2 and CO_2 environment shows that Pd and Pt based core/shell NWs have potential as a gas sensor. These core-shell nanowires with tunable transport properties show a potential for applications as electron connectors in nanoelectronic devices as well as nano gas detector for detecting O_2 gas.

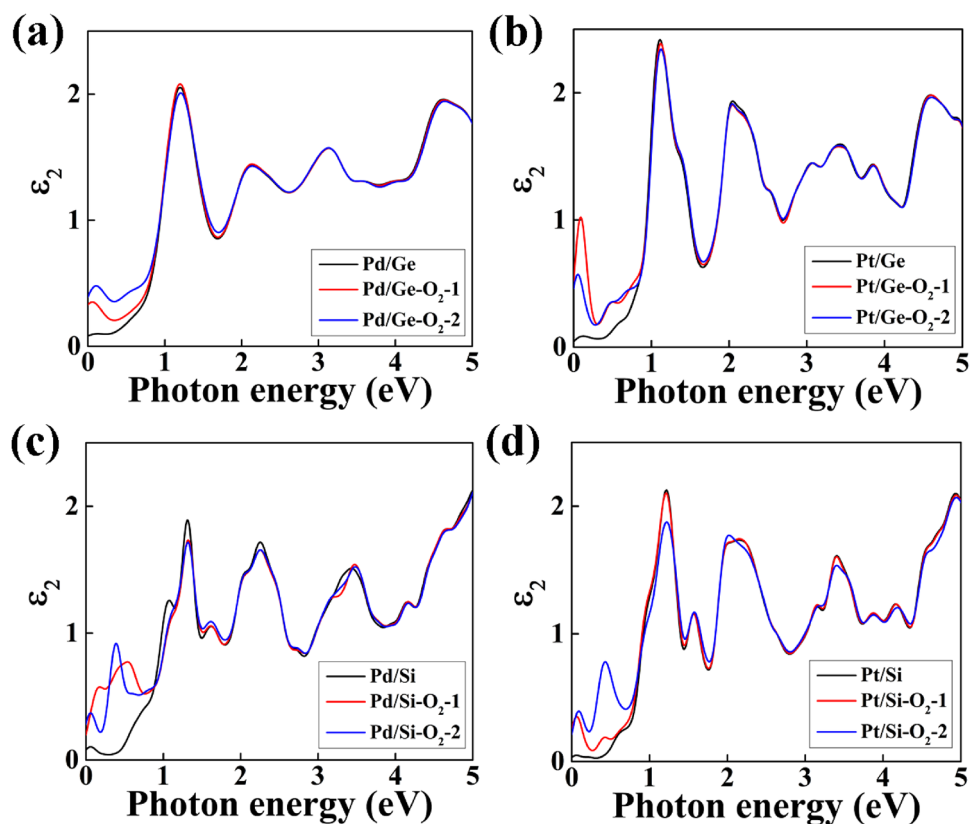


Figure 10. Variation of imaginary part (ϵ_2) of the dielectric function between the O_2 adsorbed (a) Pd/Ge, (b) Pt/Ge, (c) Pd/Si and (d) Pt/Si NW and their corresponding pure NW.

Data availability

The authors declare that all data supporting the findings of this study are available within the paper and its supplementary information files.

Received: 22 September 2020; Accepted: 9 December 2020

Published online: 11 January 2021

References

- Tang, X., Du, A. & Kou, L. Gas sensing and capturing based on two-dimensional layered materials: Overview from theoretical perspective. *WIREs Comput. Mol. Sci.* **8**, e1361 (2018).
- Jin, C. *et al.* A Janus MoSSe monolayer: A superior and strain-sensitive gas sensing material. *J. Mater. Chem. A* **7**, 1099–1106 (2019).
- Yang, D. *et al.* Gas sensor by direct growth and functionalization of metal oxide/metal sulfide core-shell nanowires on flexible substrates. *ACS Appl. Mater. Interfaces* **11**, 24298–24307 (2019).
- Chen, X., Wong, C. K. Y., Yuan, C. A. & Zhang, G. Nanowire-based gas sensors. *Sens. Actuators B Chem.* **177**, 178–195 (2013).
- Liu, Z. & Searson, P. C. Single nanoporous gold nanowire sensors. *J. Phys. Chem. B* **110**, 4318–4322 (2006).
- Murray, B. J., Walter, E. C. & Penner, R. M. Amine vapor sensing with silver mesowires. *Nano Lett.* **4**, 665–670 (2004).
- Im, Y. *et al.* Investigation of a single Pd nanowire for use as a hydrogen sensor. *Small* **2**, 356–358 (2006).
- Kyungtae, K., Cho, S.M. Pd nanowire sensors for hydrogen detection. in *2004 IEEE SENSORS 705–707* vol.2 (2004). <https://doi.org/10.1109/ICSENS.2004.1426264>.
- Miranda, A., de Santiago, F., Pérez, L. A. & Cruz-Irisson, M. Silicon nanowires as potential gas sensors: A density functional study. *Sens. Actuators B Chem.* **242**, 1246–1250 (2017).
- Cui, Y. & Lieber, C. M. Functional nanoscale electronic devices assembled using silicon nanowire building blocks. *Science* **291**, 851–853 (2001).
- Kim, N.-H. *et al.* Highly sensitive and selective hydrogen sulfide and toluene sensors using Pd functionalized WO_3 nanofibers for potential diagnosis of halitosis and lung cancer. *Sens. Actuators B Chem.* **193**, 574–581 (2014).
- Ahn, J.-H., Yun, J., Choi, Y.-K. & Park, I. Palladium nanoparticle decorated silicon nanowire field-effect transistor with side-gates for hydrogen gas detection. *Appl. Phys. Lett.* **104**, 013508 (2014).
- Kolmakov, A. & Moskovits, M. Chemical sensing and catalysis by one-dimensional metal-oxide nanostructures. *Annu. Rev. Mater. Res.* **34**, 151–180 (2004).
- Liu, D., Lin, L., Chen, Q., Zhou, H. & Wu, J. Low power consumption gas sensor created from silicon nanowires/ TiO_2 core-shell heterojunctions. *ACS Sens.* **2**, 1491–1497 (2017).
- Huang, X. & Zheng, N. One-pot, high-yield synthesis of 5-fold twinned Pd nanowires and nanorods. *J. Am. Chem. Soc.* **131**, 4602–4603 (2009).
- Lu, Y., Du, S. & Steinberger-Wilckens, R. Temperature-controlled growth of single-crystal Pt nanowire arrays for high performance catalyst electrodes in polymer electrolyte fuel cells. *Appl. Catal. B Environ.* **164**, 389–395 (2015).

17. Atashbar, M. Z. & Singamaneni, S. Room temperature gas sensor based on metallic nanowires. *Sens. Actuators B Chem.* **111–112**, 13–21 (2005).
18. Yoo, H.-W., Cho, S.-Y., Jeon, H.-J. & Jung, H.-T. Well-defined and high resolution Pt nanowire arrays for a high performance hydrogen sensor by a surface scattering phenomenon. *Anal. Chem.* **87**, 1480–1484 (2015).
19. Du, S. Pt-based nanowires as electrocatalysts in proton exchange fuel cells. *Int. J. Low-Carbon Technol.* **7**, 44–54 (2012).
20. Soler, J. M. *et al.* The SIESTA method for ab initio order- N materials simulation. *J. Phys. Condens. Matter* **14**, 2745 (2002).
21. Perdew, J. P. *et al.* Restoring the density-gradient expansion for exchange in solids and surfaces. *Phys. Rev. Lett.* **100**, 136406 (2008).
22. Troullier, N. & Martins, J. L. Efficient pseudopotentials for plane-wave calculations. *Phys. Rev. B* **43**, 1993–2006 (1991).
23. Papior, N., Lorente, N., Frederiksen, T., García, A. & Brandbyge, M. Improvements on non-equilibrium and transport Green function techniques: The next-generation transiesta. *Comput. Phys. Commun.* **212**, 8–24 (2017).
24. Datta, S. *Electronic Transport in Mesoscopic Systems* (Cambridge University Press, Cambridge, 1997).
25. Lee, H. & Choi, H. J. Single-impurity scattering and carrier mobility in doped Ge/Si core-shell nanowires. *Nano Lett.* **10**, 2207–2210 (2010).
26. Kansara, S., Gupta, S. K., Sonvane, Y. & Kumar, A. Free-standing Pt and Pd nanowires: Strain-modulated stability and magnetic and thermoelectric properties. *Phys. Chem. Chem. Phys.* **20**, 28114–28123 (2018).
27. Huang, Q., Lilley, C. M. & Bode, M. Surface scattering effect on the electrical resistivity of single crystalline silver nanowires self-assembled on vicinal Si (001). *Appl. Phys. Lett.* **95**, 103112 (2009).
28. Kamalakar, M. V. & Raychaudhuri, A. K. Low temperature electrical transport in ferromagnetic Ni nanowires. *Phys. Rev. B* **79**, 205417 (2009).
29. Bhuyan, P. D. *et al.* Si and Ge based metallic core/shell nanowires for nano-electronic device applications. *Sci. Rep.* **8**, 16885 (2018).
30. Bhuyan, P. D., Gupta, S. K., Sonvane, Y. & Gajjar, P. N. Quantum transport properties of Ni/Si nanowire for nano-electronic device application. *AIP Conf. Proc.* **2115**, 030444 (2019).
31. Huan, H., Chen, L. & Ye, X. Strain effect on the electronic and optical properties of CdSe nanowires. *Nanoscale Res. Lett.* **12**, 178 (2017).
32. N, L. Room temperature gas sensing with ultrathin Au nanowires. *J. Mater. Sci. Eng.* **5**, 2 (2016).
33. Guo, H. *et al.* CO₂ capture on h-BN sheet with high selectivity controlled by external electric field. *J. Phys. Chem. C* **119**, 6912–6917 (2015).

Acknowledgement

P.D.B. and S.K.G. would like to thank Science and Engineering Research Board (SERB), India for the financial support (Grant no.: YSS/2015/001269). P.N.G. is thankful to the Department of Science and Technology, India for the support under DST-FIST and the University Grants Commission, India for the support under DRS-SAP. RA would like to acknowledge financial support from the Swedish Research Council (VR-2016-06014). SNIC and HPC2N are also acknowledged for providing computing time.

Author contributions

P.D.B. and S.K.G. were associated with the DFT calculations and wrote the manuscript. R.A. and P.N.G. helped to improve the scientific content of the article. All authors reviewed the manuscript.

Competing interests

The authors declare no competing interests.

Additional information

Supplementary Information The online version contains supplementary material available at <https://doi.org/10.1038/s41598-020-79921-8>.

Correspondence and requests for materials should be addressed to S.K.G. or P.N.G.

Reprints and permissions information is available at www.nature.com/reprints.

Publisher's note Springer Nature remains neutral with regard to jurisdictional claims in published maps and institutional affiliations.



Open Access This article is licensed under a Creative Commons Attribution 4.0 International License, which permits use, sharing, adaptation, distribution and reproduction in any medium or format, as long as you give appropriate credit to the original author(s) and the source, provide a link to the Creative Commons licence, and indicate if changes were made. The images or other third party material in this article are included in the article's Creative Commons licence, unless indicated otherwise in a credit line to the material. If material is not included in the article's Creative Commons licence and your intended use is not permitted by statutory regulation or exceeds the permitted use, you will need to obtain permission directly from the copyright holder. To view a copy of this licence, visit <http://creativecommons.org/licenses/by/4.0/>.

© The Author(s) 2021